

23. PHYSICAL PROPERTY RELATIONSHIPS FROM SITES 765 AND 766¹

N. R. Brereton²

ABSTRACT

During Ocean Drilling Program Leg 123, two sites were drilled in the deep Indian Ocean. Physical properties were measured in soft Quaternary and Lower Cretaceous sediments to relatively fresh, glass-bearing pillow lavas and massive basalts. Porosities ranged from 89% near the seafloor to 1.6% for the dense basalts. This self-consistent set of measurements permitted some descriptive models of physical properties to be more rigorously tested than before.

Predictive relationships between porosity and compressional-wave velocity have generally been based upon the Wyllie time average equation. However, this equation does not adequately describe the actual relationship between these two parameters, and many have attempted to improve it. In most cases, models were derived by testing them against a set of data representing a relatively narrow range of porosity values. Similarly, the use of the Wyllie equation has often been justified by a pseudolinear fit to the data over a narrow range of porosity values.

The limitations of the Wyllie relationship have been re-emphasized here. A semi-empirical acoustic impedance equation is developed that provides a more accurate porosity-velocity transform, using realistic material parameters, than has hitherto been possible. A closer correlation can be achieved with this semi-empirical relationship than with more theoretically based equations. In addition, a satisfactory empirical equation can be used to describe the relationship between thermal conductivity and porosity.

If enough is known about core sample lithologies to provide estimates of the matrix and pore water parameters, then these predictive equations enable one to describe completely the behavior of a saturated rock core in terms of compressional-wave velocity, thermal conductivity, porosity, and bulk density.

INTRODUCTION

Continuous coring at Site 765 recovered a more than 930-m succession of soft Quaternary through Lower Cretaceous sediments and a further 271 m of oceanic basement with relatively fresh, glass-bearing pillow lava and massive basalt. Similar successions also were recovered from Site 766. Soon after core recovery, saturated bulk densities, grain densities, water content, porosities, compressional-wave velocities, and thermal conductivities were measured.

Preliminary results from the wide-ranging scientific investigations conducted during the Leg 123 cruise have been briefly reported (ODP Leg 123 Shipboard Scientific Party, 1989a, 1989b), and in the Leg 123 *Initial Reports* volume. More detailed findings are published here. Therefore, details of the procedures used for property measurement as well as geological descriptions of the samples will not be repeated.

PHYSICAL-PROPERTY MEASUREMENTS

Physical properties determined on board the *JOIDES Resolution* were porosity, bulk density, grain density, and water content (collectively referred to as index properties); compressional-wave velocity; and thermal conductivity. In addition, the gamma-ray attenuation porosity evaluator (GRAPE) was used to measure continuously the wet-bulk density in cores taken with the hydraulic piston corer. These, together with measurements of the undrained shear strength and other properties, will not be discussed further, but have been described in the *Initial Reports* volume for Leg 123.

Soon after core recovery, samples for determining index properties and compressional-wave velocities were taken either by cutting parallel-sided pieces with a knife in the softer sediments

or by using a double-bladed diamond saw for the more brittle or lithified sediments. Basement rock samples were obtained using a 2.5-cm rock corer. In almost all cases, these two sets of measurements were performed using the same samples. It was not practical, however, to also measure thermal conductivities for these same samples. At no time were these cores allowed to dry out prior to performing the measurement.

Index property, compressional-wave velocity, and thermal conductivity data were entered into the shipboard system, which computes the depth below seafloor (mbsf) and pertinent physical properties for each sample. A correction factor of 1.035 was necessary to bring the measured values of compressional-wave velocities into agreement with standard calibration values. Seawater velocity determined on this basis was about 1560 m/s at ambient laboratory temperature (about 25°C).

INDEX PROPERTIES

General Relationships

Index properties were determined from four measurements (wet volume, dry volume, wet mass, and dry mass), according to the following definitions:

1. Porosity (ϕ) = volume of water/volume of wet core;
2. Bulk density (ρ_s) = mass of wet core/volume of wet core;
3. Grain density (ρ_g) = mass of dry core/volume of dry core;
4. Water content (W) = mass of water/dry mass of core.

The algorithms used in the shipboard physical properties data collection system to calculate index properties were corrected for salt content by assuming a pore-water salinity of 36.3 ppt and a pore water density ($\rho\pi$) of 1.0245 g/cm³.

From these definitions, the following relationships can be derived:

$$\rho_s = \phi(\rho_p - \rho_g) + \rho_g, \quad (1)$$

¹ Gradstein, F. M., Ludden, J. N., et al., 1992. *Proc. ODP, Sci. Results*, 123: College Station, TX (Ocean Drilling Program).

² British Geological Survey, Keyworth, Nottingham, U.K.

$$W = \frac{\rho_p \phi}{\rho_g (1 - \phi)}, \quad (2)$$

$$\rho_s = \rho_p \phi \frac{(W + 1)}{W}, \quad (3)$$

$$\rho_s = \rho_g (1 - \phi)(W + 1). \quad (4)$$

Data Discrepancies

A preliminary qualitative assessment of the index properties was discussed in the *Initial Reports* volume for Leg 123, where an indication of the general stratigraphical zoning was described. All index properties determined during the cruise were tabulated.

However, while analyzing the data, it became clear that inconsistencies existed. When reducing the index properties data for the basalts and basement rocks, shipboard scientists found that in a significant number of instances, dry volume exceeded wet volume. Because this results in a grain density less than bulk density, clearly, this cannot be so. During the Leg 123 cruise, discrepancies among the wet and dry volumes were attributed to the very low porosities of the basalts, resulting in a difference less than the accuracy of the measurement. Therefore, when calculating index properties, the wet (or total) volume was determined using sample dimensions averaged with a set of calipers. This volume, along with wet and dry mass, was used to calculate index properties for the basalts and basement rocks. These results are the ones that are presented in the Leg 123 *Initial Reports* volume.

Equation 1 is a linear relationship that for a plot of ρ_s vs. ϕ should yield an intercept of ρ_g and a slope of $(\rho_p - \rho_g)$. Such a plot for all the sediment data from Sites 765 and 766 gives an intercept (i.e., grain density) of 2.899 g/cm³ and a derived value for density of pore-fluid of 1.176 g/cm³. However, the average value of the measured grain density is 2.677 g/cm³, which is close to the expected value; all the index properties have been determined on the basis of an assumed value of pore-fluid density of 1.0245 g/cm³. Thus, a discrepancy exists in the use of Equation 1 with these data.

Similarly, from Equation 3 a plot of ρ_s vs. $\phi(W + 1)/W$ should yield a value for the slope similar to a pore-fluid density of about 1.0245 g/cm³. The plot gives 1.0244 ± 0.0001 g/cm³, which is what one would expect. In addition, Equation 3 allows expected values of ρ_s to be calculated from the tabulated values of W , ϕ , and a pore-fluid density of 1.0245 g/cm³. That is, Equation 3 indicates that the relationships among ρ_s , ϕ , W , and ρ_p are correct.

The difference in the application of Equations 1 and 3 is that Equation 1 involves the use of the tabulated values of ρ_g whereas Equation 3 does not. Values of ρ_g back-calculated from Equations 1, 2, or 4 significantly differ from the tabulated values of ρ_g in a manner that seemed to indicate that an error is associated with back-calculated values of ρ_g , which is proportional to the porosity of the sample.

Relating these observations back to the measured parameters, there seemed to be no obvious discrepancies in water content values, which have been derived entirely from mass determinations. Again, no problem seems to exist with the tabulated or measured values of grain density, which have been derived from the mass determinations and from the dry volume; however, all the back-calculated values of grain density involve porosity or bulk density values, which have been derived from mass determinations, pore-fluid density (assumed to be 1.0245 g/cm³), and wet volume. I thus concluded that the measured values of wet volume, as determined by the Quantachrome helium penta-pycnometer, were in error and consequently that the tabulated values of porosity and bulk density presented in the Leg 123 *Initial Reports* volume also are in error. These errors were not revealed during

periodic checks of the accuracy of the pycnometer because calibration standards used were dry, not wet. ODP staff at Texas A&M University subsequently confirmed that a "problem" existed with the pycnometer and that this had been known for some time prior to Leg 123.

Corrections of the Data

One can rearrange the equations used for determining porosity and bulk density so that they do not use the measured values of wet volume. In this sense, the wet volume information is redundant if measured accurately, although it does allow for additional checks of data conformity.

By rearranging Equation 2, one can show that

$$\phi = \frac{W\rho_g}{(W\rho_g + 1.0245)},$$

and by substituting this into Equation 4,

$$\rho_s = 1.0245 \frac{\rho_g(W + 1)}{(W\rho_g + 1.0245)}.$$

Thus, these two equations were used to back-calculate the corrected values of porosity and bulk density that would have been determined had there been no error in wet volume. The corrected data are presented in Table 1 for Site 765 and in Table 2 for Site 766. Corrections were not applied to the basalt samples from Site 766, for which the original pycnometer-derived data were no longer available to me.

One can also show that by rearranging either of the two above equations, a plot of corrected values vs. measured values of porosity, or a plot of corrected values vs. measured values of bulk density, will yield a slope equal to the ratio of the measured value of wet volume over the value of wet volume, which would have been obtained had there been no error. For each of these two plots, the slope is 0.938 ± 0.001. That is, all measured values of porosity and bulk density were about 6.2% too high.

Index Property Correlations

A frequency histogram of grain densities for all the sediment samples from Sites 765 and 766 is shown in Figure 1. The data range from 2.16 to 3.22 g/cm³, but the average is 2.677 ± 0.134 g/cm³ with a geometric mean of 2.67 and a mode of 2.64. The cyclicity of the histogram suggests data groupings about grain density values of about 2.55, 2.64 (quartz), 2.71 (calcite), 2.75, and 2.82 g/cm³, with most falling in the quartz-calcite range. Similarly, the data range of grain densities for all the basalt samples lies between 2.66 and 2.97 g/cm³, with an average of 2.872 ± 0.064 g/cm³, a geometric mean of 2.87, and a mode of 2.85.

Earlier, I showed that a plot of ρ_s vs. ϕ should yield an intercept of ρ_g and a slope of $(\rho_p - \rho_g)$. Such a plot for all the sediment and basalt samples is shown in Figure 2. A linear regression through the sediments gives an equivalent grain density of 2.667 ± 0.017 g/cm³ and a pore-fluid density of 1.034 g/cm³ (slope = -1.633 ± 0.032). A similar regression through the basalts gives an equivalent grain density of 2.876 ± 0.008 g/cm³ and a pore-fluid density of 0.967 g/cm³ (slope = -1.909 ± 0.063). The two lines drawn through the data in Figure 2 are based upon a pore-fluid density of 1.0245 g/cm³ and grain densities of 2.872 and 2.677 g/cm³ for the upper and lower lines, respectively.

POROSITY TO VELOCITY TRANSFORMS

The now-famous Wyllie time average equation (Wyllie et al., 1956) has been universally applied to predict porosities from compressional-wave velocities, or visa-versa. Application of the

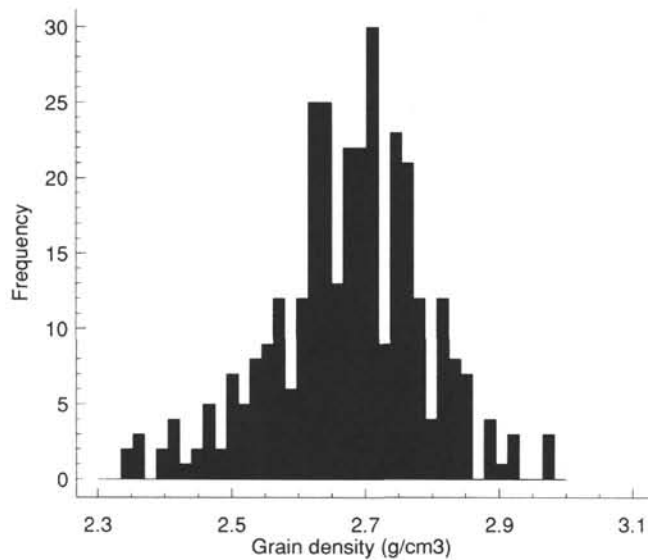


Figure 1. Histogram of sediment grain densities.

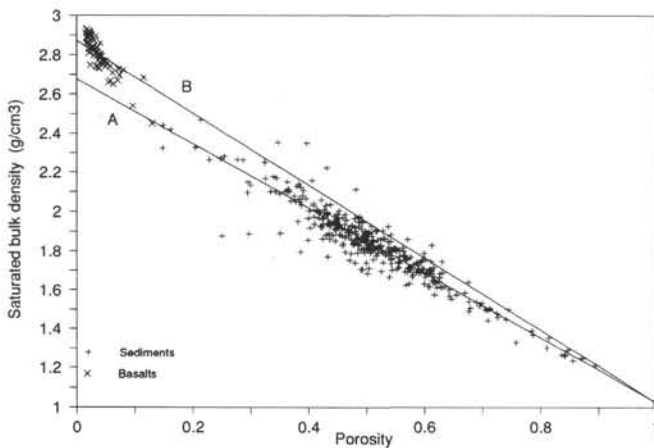


Figure 2. Relationships between porosity and saturated bulk density for the sediments and basalts from Sites 765 and 766.

equation has ranged from routine use in petrophysical analysis of geophysical borehole logs (Schlumberger, 1972; Dresser Atlas, 1982; Hearst and Nelson, 1985) to lithology and porosity determinations (Domenico, 1984) to algorithms for calculating depth-porosity relationships and for understanding subsidence history (Stam et al., 1987).

Wyllie et al. (1956) presented the time average equation in the following form

$$\frac{1}{v} = \frac{\phi}{v_p} + \frac{(1-\phi)}{v_g}$$

which can be rewritten more conveniently as

$$\frac{1}{v} = \phi \left(\frac{1}{v_p} - \frac{1}{v_g} \right) + \frac{1}{v_g} \tag{5}$$

where v is the measured compressional-wave velocity of the sample, v_p is the pore-fluid velocity, and v_g is the matrix velocity of the solid

material. This equation, which is often presented in a modified form using traveltimes rather than velocities, represents a linear relationship between inverse velocity and porosity, where the intercept at $\phi = 0$ is the inverse of the matrix velocity and where the pore-fluid velocity can be determined from the slope. Equation 5 was empirically derived from observations of synthetic aggregates of rigid media and produced a satisfactory fit to Wyllie et al. data. A less satisfactory fit was observed when applied to rock materials (Wyllie et al., 1958), especially in the high-porosity region. The poor fit to this model, and other models discussed below, has been attributed to many factors in the subsequent literature, including increased sediment frame bulk modulus and dynamic rigidity caused by overburden pressure, temperature, and hydrostatic pressure effects (Fulthorpe and Schlanger, 1989; Gardner et al., 1974).

A plot of inverse velocity vs. porosity using the Leg 123 data is shown in Figure 3. Linear regression lines are drawn through each of the sediment and basalt data sets (lines A and B, respectively), with no preconceived assumptions other than to include the water point (velocity = 1560 m/s, in accordance with the equipment calibration). Over the full porosity range, the linearity of the data trend is not convincing, but within the range from 30% to 65% a satisfactory line can be drawn. Many porosity-velocity transform practitioners deal with somewhat amorphous clouds of data within this relatively narrow range, which probably explains why they have adhered to Wyllie's time average equation for so long. The leveling off of velocity above 65% porosity corresponds to uncompacted calcareous ooze.

A plot of velocity vs. porosity is shown in Figure 4, upon which is superimposed plots of velocity derived from Equation 5. For line A, a v_g value of 6500 m/s for sediments was chosen as being intermediate between the quartz value of 6060 m/s and the calcite value of 6650 m/s (Yale, 1985). A v_g value for basalts (line B) of 7100 m/s was taken as being representative, and in both cases a v_p value of 1560 m/s was used, as described above. One can see that these two lines do not pass through the data at all and that to force them to do so (lines C and D) requires the somewhat unrealistically low values of 5800, 6200, and 1050 m/s for the sediment and basalt matrix velocities and pore water velocity, respectively.

Scientists have long recognized that Wyllie's equation (1956) does not adequately describe the actual relationship between velocity and porosity, and many have attempted to circumvent these shortcomings. In a comprehensive review of the literature, Yale (1985) reported wide discrepancies between predicted and measured values of porosity. Han et al. (1986) noted that the time

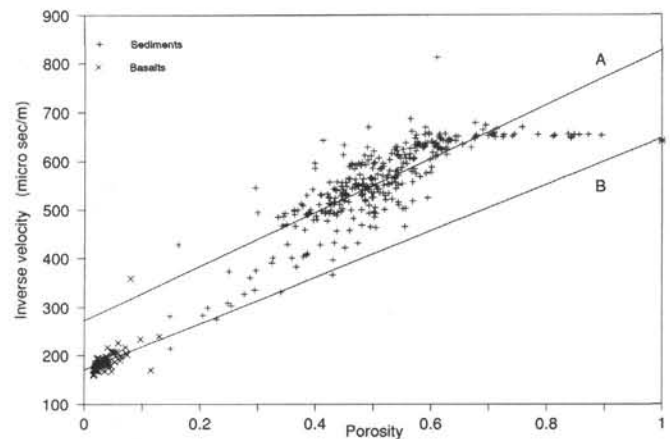


Figure 3. Linear plots of the Wyllie's time average equation.

Table 1. Index properties and velocity data, Site 765.

Core, section, interval (cm)	Depth (mbsf)	Bulk density (g/cm ³)	Grain density (g/cm ³)	Porosity (%)	Water content (%)	Velocity (m/s)
Sediments						
123-765A-1H-2, 78	2.28	1.33	2.29	75.8	139.8	1491
A-1H-4, 68	5.18	1.25	2.76	87.2	252.2	1526
A-1H-6, 68	8.18	1.44	2.46	70.9	101.4	1516
765B-1H-1, 96	0.96	1.21	2.79	89.4	311.2	1530
B-1H-3, 42	3.42	1.29	2.77	84.7	205.0	1525
B-1H-6, 61	8.11	1.23	2.48	85.5	244.5	1527
B-2H-1, 53	9.83	1.50	2.88	74.4	103.3	1523
B-2H-3, 65	12.95	1.30	2.50	81.1	175.7	1535
B-2H-6, 75	17.55	1.35	2.79	81.4	160.4	1530
B-3H-1, 83	19.63	1.45	2.66	74.1	110.0	1534
B-3H-4, 125	24.55	1.26	2.51	84.1	216.3	1544
B-3H-6, 22	26.52	1.51	2.69	71.0	93.4	1537
B-4H-2, 98	30.98	1.48	2.68	72.4	100.3	1537
B-4H-4, 115	34.15	1.39	2.73	78.5	137.0	1524
B-4H-6, 90	36.90	1.27	2.56	84.3	214.1	1535
B-5H-1, 119	39.29	1.27	2.50	83.7	209.8	1522
B-5H-4, 127	43.87	1.46	2.61	72.6	103.9	1526
B-6H-2, 102	50.32	1.49	2.63	70.7	94.2	1525
B-6H-4, 55	52.85	1.37	2.64	78.7	143.2	
B-7H-1, 113	58.53	1.52	2.65	69.5	88.0	1482
B-7H-4, 65	62.55	1.64	2.67	62.4	63.8	1521
B-7H-6, 37	65.27	1.57	2.55	64.3	72.3	1556
B-8H-2, 49	69.09	1.53	2.71	69.9	87.7	1531
B-8H-5, 42	73.52	1.55	2.52	64.6	74.3	1534
B-8H-6, 107	75.67	1.57	2.46	61.7	67.0	1543
B-9H-2, 77	79.07	1.50	2.69	71.3	94.6	1498
B-9H-3, 67	80.47	1.61	2.61	63.0	66.7	1557
B-9H-6, 36	84.66	1.54	2.62	67.6	81.7	1537
B-10H-1, 98	87.38	1.58	2.62	65.5	74.1	1575
B-10H-2, 77	88.67	1.58	2.72	67.0	76.3	1590
B-10H-6, 87	94.77	1.63	2.62	61.9	63.4	1603
B-11H-1, 62	96.62	1.60	2.64	64.2	69.7	1534
B-11H-3, 92	99.92	1.67	2.70	61.5	60.7	1547
B-11H-5, 59	102.59	1.68	2.79	62.7	61.6	1604
B-12H-2, 117	108.27	1.64	2.92	67.5	73.0	1545
B-12H-3, 77	109.37	1.69	2.82	63.1	62.1	1547
B-12H-5, 78	112.38	1.62	2.64	63.4	67.2	1552
B-13H-3, 115	119.35	1.61	2.57	62.1	65.3	1554
B-13H-5, 133	122.53	1.68	2.58	58.0	54.8	1573
B-13H-6, 77	123.47	1.74	2.75	58.6	52.7	1592
B-14H-1, 76	125.56	1.69	2.71	60.5	57.9	1572
B-14H-4, 79	130.09	1.67	2.55	57.9	55.2	1571
B-14H-5, 68	131.48	1.70	2.75	60.8	57.7	1640
B-15H-1, 100	135.50	1.76	2.86	60.2	54.1	1558
B-15H-4, 84	139.84	1.69	2.64	59.0	55.8	1568
B-15H-6, 104	143.04	1.68	2.68	60.3	58.0	1618
B-16H-1, 28	144.48	1.66	2.73	62.6	62.7	1591
B-16H-3, 80	148.00	1.62	2.54	60.9	62.7	1574
B-16H-6, 50	152.20	1.62	2.53	60.6	62.3	1586
B-17H-1, 68	154.58	1.71	2.63	57.2	52.0	1580
B-17H-4, 80	159.20	1.75	2.80	59.4	53.5	1567
B-18H-2, 47	165.57	1.75	2.97	62.9	58.6	1565
B-18H-4, 97	168.47	1.63	2.45	57.3	56.2	1609
B-18H-6, 134	171.84	1.75	2.88	61.0	55.7	1593
B-19X-1, 40	173.70	1.64	2.62	61.5	62.5	1522
B-19X-2, 67	175.47	1.69	2.73	61.2	59.3	1588
B-19X-4, 123	179.03	1.85	2.82	54.1	42.8	1610
B-20X-3, 112	187.12	1.85	2.66	49.8	38.2	
B-20X-4, 87	188.37	1.83	2.72	52.4	41.5	
B-20X-5, 90	189.90	1.70	2.75	61.1	58.6	
B-21X-1, 67	193.37	1.70	2.63	57.6	53.0	1586
B-21X-2, 60	194.80	1.77	2.78	57.6	50.1	1562
B-21X-3, 137	197.07	1.80	2.80	56.3	47.2	1596
B-22X-2, 80	204.70	1.69	2.64	58.6	55.0	1577
B-22X-3, 87	206.27	1.80	2.76	55.1	45.6	1601
B-22X-4, 60	207.50	1.83	2.67	51.2	40.2	
B-23X-1, 31	212.41	1.78	2.65	53.8	45.0	1588
B-23X-2, 40	214.00	1.71	2.36	49.0	41.7	1590
B-24X-1, 64	222.44	1.76	2.63	54.1	46.0	1628
B-24X-2, 128	224.58	1.79	2.93	59.9	52.3	
B-24X-4, 85	227.15	1.80	2.61	50.9	40.7	1648
B-25X-1, 50	232.00	1.87	2.81	52.8	40.8	1657
B-26X-2, 102	243.72	1.87	2.82	53.1	41.2	1624
B-26X-3, 13	244.33	1.90	2.85	51.8	38.6	1695

Table 1 (continued).

Core, section, interval (cm)	Depth (mbsf)	Bulk density (g/cm ³)	Grain density (g/cm ³)	Porosity (%)	Water content (%)	Velocity (m/s)
Sediments (Cont.)						
123-765B-27X-1, 48	251.38	1.93	2.75	47.5	33.7	1679
B-27X-3, 64	254.54	1.81	2.61	50.3	39.7	1674
B-28X-1, 20	260.80	1.90	2.68	47.1	34.0	1691
B-28X-2, 90	263.00	1.76	2.63	54.3	46.2	1637
B-29X-1, 87	271.07	1.78	2.75	56.4	48.1	1626
B-30X-1, 35	280.25	1.69	2.72	60.8	58.5	1568
B-31X-2, 79	291.89	1.84	2.59	47.9	36.3	1693
B-31X-4, 10	294.20	1.91	2.85	51.6	38.3	1755
B-32X-1, 45	299.75	1.89	2.76	50.1	37.2	1679
B-32X-3, 29	302.59	1.91	2.69	46.7	33.4	1711
B-33X-1, 111	310.11	1.94	2.83	49.1	34.9	1660
B-33X-4, 84	314.34	1.92	2.78	48.7	35.0	1688
B-34X-1, 89	319.59	1.92	2.75	48.1	34.5	1673
B-34X-1, 98	319.68	1.92	2.75	48.1	34.5	
B-35X-1, 110	329.40	1.98	2.81	46.3	31.4	1679
B-36X-2, 40	339.80	1.94	2.69	44.8	30.9	1631
B-37X-1, 42	347.92	1.97	2.77	45.8	31.3	1696
B-37X-CC, 56	350.43	2.06	2.71	38.4	23.6	2460
B-38X-1, 103	358.13	1.94	2.72	46.2	32.4	1688
B-38X-CC, 10	358.70	1.89	2.76	50.2	37.4	2062
B-39X-1, 32	367.02	1.83	2.64	50.4	39.5	
765C-2R-1, 80	360.40	1.99	2.72	43.2	28.6	1839
C-2R-3, 47	363.07	2.25	2.84	32.4	17.3	2559
C-3R-1, 25	369.55	1.86	2.76	51.9	40.1	1998
C-3R-1, 111	370.41	1.93	2.66	44.5	30.9	1823
C-3R-2, 25	371.05	1.85	2.52	44.6	32.7	1799
C-3R-2, 40	371.20	1.82	2.69	52.1	41.5	1923
C-4R-1, 35	379.35	1.86	2.67	49.0	36.9	1830
C-4R-1, 118	380.18	2.28	2.71	25.4	12.9	3296
C-4R-2, 84	381.34	1.89	2.76	50.3	37.5	1980
C-4R-3, 58	382.58	2.10	2.66	34.2	20.0	2141
C-5R-1, 78	389.38	1.95	2.85	49.2	34.8	1845
C-5R-3, 28	391.88	1.89	2.66	46.9	34.0	1779
C-5R-3, 78	392.38	1.89	2.78	50.4	37.5	2161
C-6R-1, 89	399.19	2.06	2.81	42.2	26.6	1903
C-6R-3, 34	401.64	1.75	2.40	47.0	37.9	1814
C-6R-3, 45	401.75	1.83	2.66	50.7	39.6	1746
C-6R-3, 70	402.00	2.03	2.72	40.8	26.0	2336
C-7R-1, 109	409.09	1.93	2.64	43.7	30.1	1793
C-7R-2, 106	410.56	2.27	2.68	24.8	12.6	3228
C-7R-3, 34	411.34	1.83	2.57	47.7	36.3	1747
C-8R-1, 49	418.19	1.88	2.72	49.6	37.0	1766
C-8R-2, 133	420.53	2.26	2.63	22.8	11.5	3624
C-8R-3, 22	420.92	1.85	2.71	51.2	39.6	
C-8R-4, 22	422.42					2134
C-8R-4, 71	422.91	1.94	2.57	41.0	27.7	1886
C-9R-1, 59	427.89	1.74	2.63	55.5	48.5	2148
C-9R-2, 112	429.92	1.78	2.58	51.6	42.4	1679
C-9R-3, 40	430.70	2.09	2.54	29.4	16.8	2979
C-9R-5, 60	433.90	1.76	2.52	51.1	42.5	1714
C-10R-2, 30	438.30	1.72	2.58	55.5	49.6	1990
C-10R-2, 47	438.47	1.96	2.65	42.4	28.5	1796
C-10R-4, 33	441.33	1.87	2.71	49.7	37.4	1906
C-10R-4, 112	442.12					1650
C-11R-1, 111	447.11	1.89	2.60	45.4	32.7	1825
C-11R-2, 91	448.41	2.26	2.76	28.6	14.9	2776
C-11R-3, 110	450.10	2.13	2.80	37.9	22.3	2475
C-11R-4, 116	451.66	1.62	2.61	62.7	66.0	1629
C-12R-1, 68	455.88	1.96	2.77	46.5	32.2	2075
C-12R-3, 85	459.05	2.10	2.72	36.3	21.5	2040
C-12R-4, 36	460.06	2.05	2.69	38.5	23.8	1887
C-12R-5, 67	461.87	1.93	2.63	43.7	30.2	2193
C-13R-1, 96	465.56	2.44	2.69	15.0	6.7	4670
C-13R-2, 127	467.37	2.08	2.75	38.9	23.7	2021
C-13R-3, 10	467.70	1.91	2.67	46.2	32.9	2003
C-14R-1, 59	474.69	1.99	2.73	43.2	28.5	1958
C-15R-1, 17	483.87	1.71	2.64	57.4	52.2	1741
C-16R-1, 103	494.23	2.11	3.12	48.2	30.5	1879
C-16R-2, 24	494.94					1871
C-16R-4, 50	498.20	2.35	3.06	34.7	17.8	2031
C-17R-1, 133	503.73	1.93	2.67	45.2	31.7	1800
C-17R-2, 109	504.99	1.84	2.63	48.9	37.3	
C-17R-3, 40	505.80	2.04	2.74	40.8	25.8	1882
C-18R-1, 78	512.68	1.86	2.51	43.6	31.5	1854

Table 1 (continued).

Core, section, interval (cm)	Depth (mbsf)	Bulk density (g/cm ³)	Grain density (g/cm ³)	Porosity (%)	Water content (%)	Velocity (m/s)
Sediments (Cont.)						
123-765C-18R-2, 48	513.88	1.81	2.64	51.4	41.0	1708
C-18R-3, 40	515.30	1.99	2.72	43.3	28.8	1907
C-19R-1, 55	521.85	1.87	2.66	48.5	36.2	1827
C-19R-2, 81	523.61	1.91	2.89	52.8	39.6	1808
C-19R-3, 119	525.49	1.94	2.65	43.6	29.9	2048
C-20R-1, 50	531.30	2.03	2.67	38.8	24.3	2033
C-20R-1, 94	531.74	2.14	2.83	38.3	22.5	2039
C-20R-2, 71	533.01	1.79	2.47	47.3	37.2	1823
C-21R-1, 15	540.55	2.11	2.80	39.1	23.5	2000
C-22R-1, 61	550.71	1.87	2.60	46.3	34.0	
C-22R-1, 148	551.58	2.05	2.65	36.9	22.6	2004
C-22R-2, 102	552.62	1.81	2.56	49.0	38.5	1842
C-23R-4, 3	564.23	2.13	2.61	30.0	16.8	2023
C-23R-5, 3	565.73	2.10	2.64	33.4	19.5	2063
C-24R-1, 40	569.70	2.15	2.79	36.3	20.9	2010
C-24R-1, 146	570.76	2.10	2.71	36.3	21.5	2001
C-24R-3, 4	572.34	2.35	3.22	39.6	20.9	2091
C-25R-1, 37	579.37	2.17	2.77	34.4	19.4	2059
C-25R-3, 62	582.62	2.08	2.71	37.5	22.7	1952
C-25R-5, 19	585.19	2.05	2.67	37.8	23.3	1968
C-26R-4, 34	593.04	1.76	2.73	56.9	49.5	1655
C-26R-5, 37	594.12	1.71	2.55	55.2	49.5	1677
C-27R-1, 45	597.95	1.70	2.75	61.1	58.5	1632
C-27R-2, 18	599.25	1.74	2.63	55.7	48.9	1650
C-28R-1, 85	607.85	1.77	2.71	55.7	47.6	1680
C-28R-2, 97	609.47	1.81	2.71	53.6	43.7	1771
C-29R-1, 82	617.22	1.83	2.65	50.3	39.1	1775
C-29R-5, 35	622.97	1.82	2.59	49.5	38.7	1769
C-29R-6, 10	624.27	1.88	2.76	50.9	38.5	
C-30R-2, 56	627.95	1.88	2.73	49.8	37.2	1781
C-30R-4, 107	631.39	1.74	2.58	54.3	47.1	1753
C-30R-6, 80	634.09	1.90	2.84	51.6	38.5	1868
C-31R-1, 3	635.33	2.32	2.55	14.8	7.0	3549
C-31R-2, 74	637.45	1.93	2.67	44.8	31.1	1863
C-31R-3, 138	639.56	1.93	2.69	45.3	31.6	1882
C-32R-1, 77	645.77	1.96	2.72	44.8	30.6	1848
C-35R-1, 127	675.37	1.79	2.51	48.4	38.3	1823
C-35R-2, 94	676.54	1.83	2.59	48.6	37.4	1933
C-35R-3, 78	677.88	1.74	2.40	48.0	39.4	1890
C-35R-4, 41	679.01	1.80	2.46	46.3	35.9	1841
C-36R-2, 10	684.90	1.77	2.34	43.3	33.4	2315
C-36R-5, 120	690.50	1.84	2.53	45.9	34.4	1777
C-36R-6, 45	691.25	1.86	2.41	39.9	28.2	1676
C-37R-1, 107	694.07	1.70	2.51	54.4	48.6	1959
C-37R-2, 62	695.12	2.00	2.81	45.2	30.1	1888
C-37R-3, 96	696.96	1.93	2.58	42.0	28.8	1876
C-38R-1, 142	703.92	1.92	2.58	42.3	29.1	1949
C-38R-3, 47	705.97	1.80	2.28	38.6	28.2	2438
C-38R-5, 104	709.54	1.86	2.48	42.4	30.4	2035
C-38R-7, 7	711.57	1.88	2.60	45.7	33.2	1938
C-39R-1, 82	712.52	1.91	2.62	44.7	31.6	1876
C-39R-3, 51	715.21	1.71	2.41	50.3	43.1	2031
C-40R-2, 124	723.64	1.97	2.64	41.7	27.8	2017
C-40R-4, 22	725.62	1.90	2.79	50.5	37.4	1823
C-41R-1, 9	730.49	2.01	2.70	41.3	26.7	1553
C-42R-1, 46	740.26	1.86	2.62	47.9	36.0	1888
C-42R-2, 15	741.45	1.99	2.77	45.0	30.2	1578
C-42R-4, 59	744.89	1.91	2.77	49.1	35.7	1491
C-43R-2, 121	751.81	1.86	2.72	50.9	39.1	
C-43R-4, 138	754.98	1.86	2.63	48.2	36.3	1776
C-43R-6, 52	757.12	1.90	2.77	49.8	36.7	1808
C-44R-2, 91	760.91	1.85	2.81	53.7	42.3	1762
C-44R-4, 34	763.34	2.42	2.69	16.3	7.4	2338
C-45R-1, 92	769.12	1.91	2.69	46.9	33.6	1829
C-45R-5, 70	774.90	1.89	2.69	48.1	35.3	1806
C-46R-1, 41	778.21	1.89	2.75	49.8	36.9	1772
C-46R-2, 36	779.66	1.97	2.86	48.5	33.8	1850
C-47R-1, 112	788.52	1.92	2.75	48.1	34.5	1848
C-47R-4, 32	792.22	1.92	2.67	45.7	32.3	1770
C-48R-1, 86	797.76	2.22	3.13	43.1	24.8	2028
C-48R-6, 127	805.67	2.01	2.74	42.6	27.8	1957
C-49R-1, 98	807.28	1.94	2.61	42.5	29.0	1907
C-49R-4, 82	811.62	1.94	2.64	43.4	29.7	1938
C-50R-2, 90	818.00	1.94	2.63	43.2	29.6	1941

Table 1 (continued).

Core, section, interval (cm)	Depth (mbsf)	Bulk density (g/cm ³)	Grain density (g/cm ³)	Porosity (%)	Water content (%)	Velocity (m/s)
Sediments (Cont.)						
123-765C-50R-5, 38	821.98	2.16	2.93	40.6	23.9	1957
C-51R-1, 35	825.35	1.93	2.67	45.0	31.4	1929
C-51R-5, 5	831.05	2.00	2.66	40.1	25.8	2053
C-52R-2, 12	836.12	2.03	2.82	43.8	28.3	2023
C-52R-3, 102	838.52	1.98	2.74	44.4	29.9	2013
C-53R-1, 29	844.39	1.88	2.53	43.0	30.6	2520
C-53R-4, 26	848.86	2.17	2.72	32.6	18.2	2492
C-53R-7, 37	853.47	1.92	2.52	40.3	27.4	2084
C-54R-1, 109	854.59	2.00	2.70	41.7	27.1	2029
C-54R-4, 90	858.90	1.95	2.52	38.2	25.1	2181
C-55R-1, 107	864.07	1.95	2.70	44.6	30.6	1991
C-55R-3, 82	866.82	2.12	2.81	38.6	22.9	2044
C-56R-1, 67	873.17	2.00	2.70	42.0	27.5	2097
C-56R-2, 94	874.94	1.98	2.69	42.6	28.3	2003
C-57R-1, 6	881.76	1.94	2.68	44.7	30.9	1923
C-57R-3, 69	885.39	2.11	2.74	36.5	21.5	2147
C-58R-1, 90	892.10	2.09	2.66	35.0	20.7	2129
C-58R-4, 40	896.10	1.97	2.63	40.9	27.0	2010
Basalts						
C-63R-2, 23	937.47	2.75	2.85	5.3	2.0	5341
C-63R-4, 133	941.54	2.76	2.85	4.8	1.8	5952
C-64R-1, 48	945.78	2.65	2.76	6.3	2.5	5067
C-65R-1, 27	954.97	2.86	2.89	1.7	0.6	6267
C-65R-2, 40	956.50	2.71	2.82	6.2	2.4	5260
765D-1R-1, 113	949.03	2.77	2.85	4.5	1.7	5578
D-2R-2, 31	956.40	2.93	2.96	1.7	0.6	6148
D-2R-3, 88	958.04	2.75	2.79	2.4	0.9	5893
D-3R-1, 35	964.75	2.79	2.86	4.0	1.5	5495
D-5R-1, 16	983.36	2.80	2.86	3.5	1.3	5552
D-5R-1, 118	984.38	2.83	2.90	3.5	1.3	5952
D-5R-5, 61	988.77	2.81	2.88	3.5	1.3	5292
D-6R-2, 30	994.20	2.72	2.87	8.0	3.1	2785
D-7R-1, 138	1003.38	2.92	2.96	2.3	0.8	5936
D-7R-2, 122	1004.68	2.70	2.83	7.4	2.9	4955
D-7R-3, 48	1005.36	2.73	2.86	7.2	2.8	4883
D-8R-1, 37	1011.87	2.80	2.88	4.0	1.5	5550
D-9R-1, 38	1021.28	2.83	2.87	2.2	0.8	5859
D-9R-3, 17	1024.01	2.87	2.93	3.0	1.1	5563
D-10R-1, 116	1031.36	2.76	2.83	4.0	1.5	5551
D-11R-1, 45	1039.85	2.88	2.92	2.0	0.7	5792
D-12R-1, 55	1045.65	2.73	2.80	3.7	1.4	5160
D-13R-1, 18	1054.58	2.73	2.80	3.9	1.5	5073
D-14R-1, 9	1063.99	2.89	2.93	2.0	0.7	5410
D-15R-2, 26	1074.76	2.83	2.88	2.5	0.9	5377
D-16R-1, 58	1083.08	2.81	2.85	2.2	0.8	5528
D-17R-3, 13	1094.67	2.77	2.86	5.0	1.9	4903
D-18R-1, 99	1102.09	2.90	2.94	2.0	0.7	5907
D-18R-3, 78	1103.92	2.77	2.84	3.7	1.4	5041
D-19R-1, 98	1111.28	2.74	2.83	5.0	1.9	4814
D-19R-2, 38	1111.98	2.79	2.87	4.3	1.6	5481
D-20R-1, 47	1119.97	2.80	2.85	3.0	1.1	5194
D-21R-1, 86	1129.86	2.74	2.80	3.4	1.3	5193
D-22R-1, 96	1139.56	2.67	2.77	5.9	2.3	4406
D-23R-2, 65	1149.95	2.80	2.87	4.0	1.5	4598
D-24R-1, 13	1157.23	2.83	2.88	2.7	1.0	5669
D-24R-3, 33	1160.00	2.90	2.96	3.4	1.2	5284
D-24R-4, 95	1161.85	2.68	2.90	11.5	4.6	5883
D-25R-2, 11	1168.04	2.86	2.90	1.9	0.7	5675
D-26R-1, 28	1176.28	2.83	2.90	3.5	1.3	5349

average equation significantly overestimates velocities and found it necessary to use unrealistically low values of matrix velocity to accommodate a fit with the data.

Wilkens et al. (1986) used aspect ratio modeling to describe the effect of varying clay content on the porosity-velocity relationship; Castagna et al. (1985), Han et al. (1986), Taylor-Smith

(1974), and Anderson (1974) fitted least-squares empirical equations to their data to derive linear relationships among velocity, porosity, and clay content; and Rafavich et al. (1984) developed linear relationships involving a wide range of petrographic characteristics. The drawback of this approach is that the coefficients derived to fit the empirical equations are specific to the rock

Table 2. Index properties and velocity data, Site 766.

Core, section, interval (cm)	Depth (mbsf)	Bulk density (g/cm ³)	Grain density (g/cm ³)	Porosity (%)	Water content (%)	Velocity (m/s)
Sediments						
123-766A-1R-2, 30	1.80	1.50	2.64	70.4	92.3	1521
A-1R-3, 39	3.39	1.51	2.53	67.9	85.5	1529
A-2R-2, 60	9.86	1.54	2.68	69.0	84.9	1503
A-2R-7, 21	16.97	1.49	2.46	67.6	87.0	1471
A-3R-1, 10	17.40	1.65	2.64	61.3	61.5	1534
A-3R-4, 35	22.15	1.80	2.78	55.6	46.1	1568
A-4R-1, 129	28.29	1.71	2.71	59.6	55.7	1515
A-4R-2, 105	29.55	1.77	2.74	56.4	48.4	1455
A-5R-2, 97	39.17	1.74	2.76	58.9	53.2	1525
A-5R-5, 70	43.40	1.71	2.63	57.2	52.1	1544
A-7R-4, 56	61.06	1.75	2.83	59.6	53.5	1526
A-7R-6, 118	64.68	1.72	2.65	57.4	52.1	1528
A-8R-1, 50	66.20	1.69	2.57	56.7	52.1	1510
A-9R-1, 47	75.77	1.73	2.73	58.9	53.7	1587
A-9R-4, 94	80.74	1.70	2.68	59.0	55.1	1492
A-11R-1, 133	96.03	1.79	2.55	49.6	39.5	1637
A-11R-4, 51	99.71	1.83	2.59	48.5	37.2	1634
A-12R-1, 35	104.65	1.81	2.59	50.1	39.7	1611
A-13R-2, 13	115.53	1.71	2.82	61.6	58.2	1595
A-13R-3, 116	118.06	1.74	2.64	55.4	48.3	1631
A-14R-2, 50	125.60	1.86	2.97	57.1	45.9	1647
A-14R-4, 120	129.30	1.82	2.77	54.7	44.6	1649
A-15R-6, 20	140.90	1.71	2.77	61.0	57.8	1230
A-16R-1, 52	143.42	1.83	3.10	61.2	52.2	1592
A-16R-3, 67	146.57	1.88	2.90	54.1	41.7	1589
A-16R-5, 43	149.33	1.93	2.97	53.7	40.0	1601
A-17R-2, 106	155.06	1.80	2.72	54.3	44.8	1633
A-17R-5, 111	159.61	1.82	2.83	56.2	46.4	1647
A-18R-2, 146	165.06	1.78	2.76	56.6	48.5	1727
A-18R-4, 14	166.74	1.74	2.54	52.8	45.1	1723
A-18R-6, 33	169.93	1.90	2.67	47.0	34.0	1811
A-19R-1, 38	172.08	1.75	2.71	56.8	49.7	1930
A-19R-3, 131	176.01	1.79	2.70	54.1	44.8	1719
A-19R-5, 21	177.91	1.81	2.76	54.9	45.1	1704
A-20R-1, 17	181.57	1.93	2.74	47.4	33.7	1817
A-20R-3, 11	184.51	2.15	2.62	29.5	16.4	1834
A-21R-11, 6	191.16	1.89	2.56	43.5	30.8	1846
A-21R-2, 90	193.40	1.88	2.64	46.9	34.3	1806
A-22R-1, 25	200.85	1.89	2.25	29.7	19.2	2664
A-23R-1, 29	210.59	1.88	2.56	44.2	31.7	1957
A-24R-1, 53	220.43	1.92	2.63	44.5	31.2	1893
A-24R-CC, 10	221.50	1.88	2.16	25.0	15.8	2679
A-25R-1, 72	230.32	1.89	2.36	35.1	23.5	2332
A-26R-1, 109	240.39	1.78	2.64	53.2	44.2	1915
A-26R-3, 35	242.65	1.69	2.35	50.1	43.8	2017
A-27R-1, 134	250.24	1.71	2.37	49.3	42.0	2028
A-27R-2, 74	251.14	1.67	2.42	53.9	49.5	1838
A-28R-2, 78	260.88	1.74	2.45	49.9	41.6	1901
A-28R-4, 83	263.93	1.69	2.58	57.0	52.7	1711
A-28R-6, 68	266.78	1.62	2.41	56.8	55.8	1793
A-29R-1, 71	269.01	1.67	2.63	60.1	58.6	1702
A-29R-3, 126	272.56	1.63	2.54	59.9	60.3	1734
A-30R-1, 12	278.02	1.70	2.68	59.1	55.3	1737
A-30R-4, 18	282.58	1.71	2.73	59.8	55.9	1656
A-31R-1, 99	288.49	1.96	2.59	39.9	26.3	1708
A-32R-1, 27	297.47	1.70	2.44	52.5	46.4	1751
A-32R-3, 3	300.23	1.83	2.51	45.9	34.6	2186
A-32R-5, 32	303.52	1.79	2.58	50.6	40.7	1840
A-33R-1, 66	307.46	1.95	2.84	49.2	35.0	1964
A-33R-3, 9	309.88	2.06	2.74	39.5	24.4	1844
A-34R-1, 18	316.68	1.86	2.69	50.1	38.2	1867
A-34R-1, 136	317.86	1.81	2.78	55.0	45.0	1807
A-36R-2, 17	337.47	1.73	2.71	58.1	52.4	1760
A-37R-2, 129	348.21	1.80	2.66	52.6	42.8	1870
A-37R-3, 18	348.60	2.10	2.70	35.8	21.2	2493
A-38R-1, 81	355.91	2.18	2.77	33.9	19.0	3017
A-38R-3, 29	358.39	1.97	2.74	45.1	30.7	2369
A-39R-2, 44	366.74	2.03	2.79	43.0	27.7	2727
A-39R-3, 40	368.20	1.80	2.73	54.3	44.5	1940
A-40R-2, 42	376.42	1.69	2.66	59.4	56.3	1906
A-40R-4, 14	379.14	1.86	2.61	47.3	35.3	2317
A-41R-1, 95	385.15	1.90	2.71	48.0	34.9	2135
A-41R-3, 39	387.59	1.75	2.62	54.3	46.4	1817
A-41R-5, 89	391.09	1.82	2.67	51.8	41.2	1816

Table 2 (continued).

Core, section, interval (cm)	Depth (mbsf)	Bulk density (g/cm ³)	Grain density (g/cm ³)	Porosity (%)	Water content (%)	Velocity (m/s)
Sediments (Cont.)						
123-766A-42R-1, 102	394.82	1.80	2.75	55.1	45.7	1991
A-42R-3, 109	397.89	2.33	2.66	20.4	9.9	3523
A-43R-1, 50	404.00	2.10	2.72	36.7	21.8	2613
A-43R-1, 65	404.15	1.82	2.75	53.8	43.4	1797
A-43R-3, 48	406.98	1.88	2.72	49.5	36.9	2150
A-43R-5, 53	410.03	1.85	2.67	49.6	37.8	1866
A-44R-1, 90	414.10	1.78	2.65	53.8	45.0	1728
A-44R-3, 98	417.18	1.86	2.70	49.8	37.7	1707
A-44R-6, 53	421.23	1.89	2.74	49.7	37.0	1773
A-45R-1, 112	423.92	1.85	2.72	51.1	39.4	1868
A-45R-3, 36	426.16	2.47	2.86	21.3	9.7	3337
A-45R-5, 29	429.09	1.96	2.83	47.9	33.3	2000
A-46R-2, 48	434.52	1.82	2.70	52.4	41.7	1766
A-46R-4, 23	437.27	2.27	2.74	27.7	14.3	3050
A-46R-6, 110	441.14	1.79	2.66	53.2	43.8	1801
A-47R-1, 121	443.41	1.93	2.86	50.8	37.0	1840
A-47R-4, 53	447.23	1.86	2.78	52.4	40.6	1809
A-48R-1, 98	452.78	1.95	2.82	48.6	34.3	1921
A-48R-3, 36	455.16	1.82	2.61	50.0	39.2	1901
A-48R-5, 78	458.58	1.79	2.62	52.0	42.3	1890
Basalts						
A-48R-7, 8	460.70	2.45	2.66	13.0	5.7	4161
A-48R-7, 61	461.23	2.67	2.80	7.1	2.8	4603
A-49R-1, 25	461.75	2.76	2.84	4.0	1.5	5179
A-49R-1, 78	462.28	2.54	2.71	9.7	4.1	4270
Sediments						
A-49R-2, 50	463.50	1.93	2.67	45.2	31.7	1874
A-49R-3, 65	465.15	1.97	2.88	48.8	33.9	1822
Basalts						
A-49R-4, 116	467.16	2.84	2.89	2.9	1.0	5451
A-49R-5, 38	467.83	2.85	2.90	2.2	0.8	5439
A-50R-1, 135	472.55	2.66	2.76	5.5	2.1	4821
A-50R-3, 112	475.14	2.77	2.85	4.6	1.7	4787
A-50R-4, 13	475.52	2.74	2.85	5.8	2.2	4877
A-51R-1, 90	481.30	2.84	2.89	2.6	0.9	5515
A-51R-5, 17	486.38	2.86	2.94	4.1	1.5	5372
A-52R-1, 25	490.15	2.88	2.93	2.8	1.0	5498
A-52R-3, 98	493.95	2.89	2.92	1.8	0.6	5740
A-52R-5, 55	496.29	2.90	2.95	2.2	0.8	5162
A-53R-1, 35	499.45	2.90	2.93	2.0	0.7	5567
A-53R-3, 52	502.22	2.91	2.95	2.1	0.7	5757
A-53R-5, 62	504.51	2.90	2.95	2.5	0.9	5730
A-53R-7, 91	507.60	2.91	2.96	2.4	0.9	5117
A-54R-2, 108	510.70	2.91	2.94	1.6	0.6	5901
A-54R-4, 96	513.22	2.93	2.97	1.8	0.6	5898
A-54R-6, 118	515.68	2.92	2.96	2.1	0.8	5730

materials for which they were determined, thereby limiting their applicability to particular formations and environments. In addition, often no physical basis exists to justify such equations.

An equally unsatisfactory approach, also of limited applicability, has been to modify the time average equation by applying a "compaction correction factor" to account for unconsolidated high-porosity materials (Collins and Pilles, 1979; Schlumberger, 1972; Dresser Atlas, 1982). Anderson (1984) simulated the effect on velocity of oil and gas saturation, but stressed that his theoretical model was applicable only under those conditions where the time average equation has been satisfied.

Pioneering work in the field of the velocity of sound in porous media was conducted by Wood (1941), who showed that for a suspension of solid particles in a liquid, the mean bulk compressibility equals the sum of the compressibilities of the individual components. From fundamental equations governing velocity

through a perfectly elastic, homogeneous, isotropic solid, Wood showed that

$$\frac{1}{\rho_s v^2} = \phi \left(\frac{1}{\rho_p v_p^2} - \frac{1}{\rho_g v_g^2} \right) + \frac{1}{\rho_g v_g^2} \tag{6}$$

Equation 6, which in another form is known as the Wood emulsion equation, represents a linear relationship between $1/\rho_s v^2$ and porosity. A plot using the Leg 123 data is shown in Figure 5, with linear regression lines drawn through each of the sediment (line A) and basalt (line B) data sets under the same assumptions as for Figure 3. The linearity of these data is a considerable improvement over the time average equation, but the plot has a significant S-shaped characteristic.

Hamilton (1971) and the McCanns (1968a, 1968b) showed that while a suspension of solid particles in a liquid can, to a certain

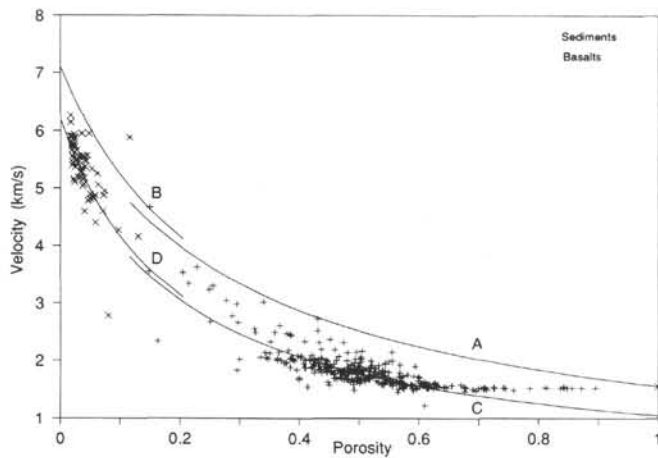


Figure 4. Wyllie's time average equation velocity/porosity predictions.

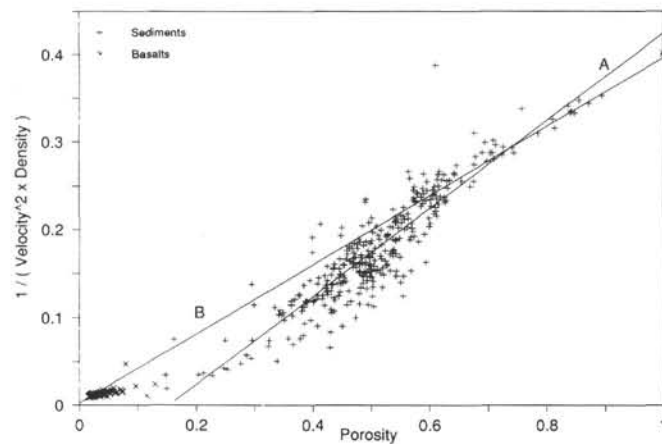


Figure 5. Linear plots of the Wood's emulsion equation.

extent, be regarded as a two-phase medium, the Wood equation simply places a lower limit on the magnitude of velocity (Buchan et al., 1971). One can readily see this in the literature where the Wood equation has been fitted to data (see Shumway, 1960; Buchan et al., 1971; Taylor-Smith, 1974; Jackson et al., 1981; and Nobes et al., 1986). Indeed, Nobes et al. (1986) found it necessary to take an empirically weighted mean of both the Wood and Wyllie equations to compute a better representation of their data over the full range of porosities of Pacific Ocean floor sediments.

To counteract this minimum limit effect, Wyllie et al. (1956) introduced the rigidity of the bulk materials and solid matrix into the Wood equation, giving the following (presented here in the form of Equation 6):

$$\frac{(1+q)}{\rho_s v^2} = \phi \left(\frac{1}{\rho_p v_p^2} - \frac{(1+q_g)}{\rho_g v_g^2} \right) + \frac{(1+q_g)}{\rho_g v_g^2}, \quad (7)$$

where

$$q = \frac{2(1-2\sigma)}{(1+\sigma)} \quad \text{and} \quad q_g = \frac{2(1-2\sigma_g)}{(1+\sigma_g)},$$

and σ = Poisson's ratio. The quantity q (or q_g) was not specifically defined by Wyllie et al. (1956), but is related to the bulk moduli of the different components and can be regarded as a rigidity index.

If q and q_g are equal, the predicted velocity approaches the matrix velocity at the lower end of the porosity range. However, an examination of Equation 7 reveals that it also has the effect of increasing the predicted velocity values, including the pore-water velocity, at the higher end of the porosity range. Clearly, Wyllie did not intend that the inclusion of shear modulus effects in the Wood equation should be applied with equal weight at both the high and low ends of the porosity range. Because the Wood equation was derived to describe loose suspensions of solid particles in a liquid, the inclusion of shear modulus effects should be at a minimum at the higher porosities, increasing progressively to a maximum at the lower porosities. This can be achieved by multiplying both q and q_g by $(1-\phi)$, so that Equation 7 becomes

$$\frac{(1+q[1-\phi])}{\rho_s v^2} = \phi \left(\frac{1}{\rho_p v_p^2} - \frac{(1+q_g[1-\phi])}{\rho_g v_g^2} \right) + \frac{(1+q_g[1-\phi])}{\rho_g v_g^2}. \quad (8)$$

A plot of velocity vs. porosity for the Leg 123 data is shown in Figure 6, upon which is superimposed a plot of sediment velocities derived from Wood's equation (Eq. 6), line A, using matrix and pore-water velocities as before, a pore-fluid density of 1.0245 g/cm³, and a grain density of 2.667 g/cm³. Bulk density values were derived from Equation 1. Although the overall curvature of this line tends to represent a minimum envelope (as described above), it actually plots through the data in the porosity range of about 62% to 100%, rather than below it. Therefore, in this porosity range, Wood's equation predicts velocity well.

Also shown in Figure 6 is a plot of velocity predicted from the modified Wyllie-Wood equation (Eq. 8) for the sediments (line B) and the basalts (line C). These are based upon sediment parameters as for line A; a basalt matrix velocity of 7100 m/s and grain density of 2.872 g/cm³, a q_g value of 0.55 derived from a Poisson's ratio of 0.32 (from velocities given in Yale, 1985); and a mean bulk q value of 0.6 derived from a Poisson's ratio of 0.3 (Wyllie et al., 1956; Domenico, 1984). Lines B and C show good correlations of the predicted with measured velocities over most of the porosity range. With unequal values for q and q_g , however, the predicted velocities approach values other than the matrix velocities when porosity approaches zero. In this case, these velocities are 6604 and 7214 m/s for the sediments and basalts, respectively.

Nafe and Drake (1957) took a slightly different approach to Wyllie et al. (1956) and considered the application of applied

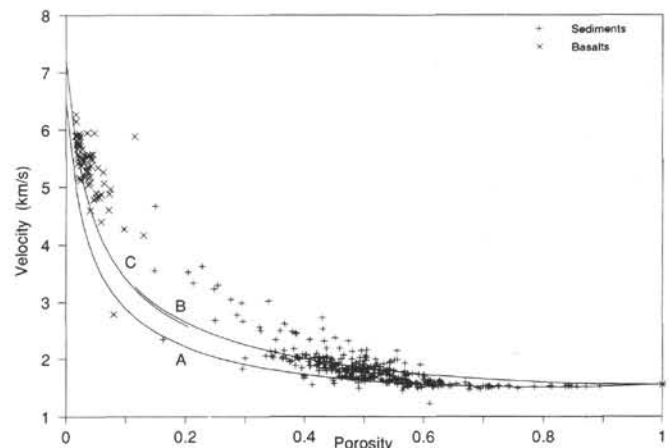


Figure 6. Wood's emulsion equation velocity/porosity predictions.

pressures to the total system. They made certain empirical assumptions and derived the following equation:

$$v = \phi v_w^2 \left(1 + \frac{\rho_p}{\rho_s} (1 - \phi) \right) + \frac{\rho_g}{\rho_s} v_g^2 (1 - \phi)^n,$$

where v_w is the velocity predicted by Wood's equation (Eq. 6) and n was suggested to lie between 4 and 5. Nafe and Drake (1957) commented that comparison of their equation with experimental data gave velocities that were too low at the higher porosities and that this could not be improved by different choices of n . This observation was confirmed by Brereton (1990), who showed that for the Leg 123 data, predicted velocities were too low over the 50% to 100% porosity range and too high over the 0% to 50% range.

More recently, in the development of porosity to velocity transforms, Raymer et al. (1980) presented three algorithms to describe the upper and lower porosity ranges separately and a linear interpolation to link the two. The first two algorithms were given as alternatives for the 0% to 37% range; but the third, to describe the 47% to 100% range, was stated to be totally empirical, but is in fact Wood's equation (though not attributed as such). Raiga-Clemenceau et al. (1988) introduced the concept of an acoustic formation factor to describe the velocity-porosity relationship in the 0% to 50% porosity range. When implemented, their empirically derived equation does not differ significantly from Raymer et al.'s algorithms. Brereton (1990) demonstrated that for the Leg 123 data, these algorithms predict consistently higher velocities than those measured, in much the same way as Wyllie's time average equation.

The well-defined data relationship between porosity and velocity led to much of the work discussed above. An equally well-defined relationship between bulk density and velocity has also long been recognized, and the use of acoustic impedance (the product of velocity and bulk density) to determine reflection coefficients is an established tool in seismic interpretation (Rafavich et al., 1984). Gardner et al. (1974) derived an empirical exponential relationship between density and velocity based upon reflection coefficient considerations. The close linearity between porosity and the reflection coefficient is relatively well documented (Buchan et al., 1971; Taylor-Smith, 1974), but does not seem to have been explored as the basis of a potential porosity-velocity transform.

Following the lead given by Wood and Wyllie et al., a plot of inverse acoustic impedance vs. porosity is shown in Figure 7 using the Leg 123 data, with linear regression lines drawn through each of the sediment (line A) and basalt (line B) data sets under

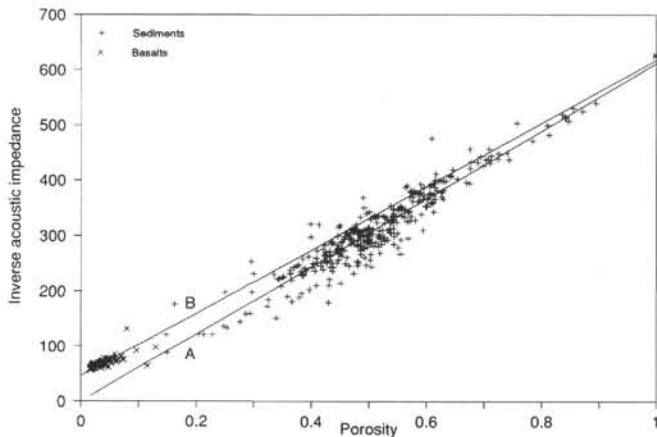


Figure 7. Linear plots of the acoustic impedance equation.

the same assumptions as for Figure 3. The linearity of these data is clear and is significantly better than that for Wood's equation (Figure 5). These linear regression lines are represented by the following equation,

$$\frac{1}{\rho_s v} = \phi \left(\frac{1}{\rho_p v_p} - \frac{1}{\rho_g v_g} \right) + \frac{1}{\rho_g v_g}. \tag{9}$$

Figure 8 depicts a plot of velocities derived from Equation 9 (line A) superimposed upon the Leg 123 velocity-porosity data using the same sediment parameters as before. For direct comparison, the velocities derived from Wood's equation (Eq. 6), are also shown in Figure 8 as line B. Clearly, while the original Wood equation is a better predictor of velocities over the 45% to 100% porosity range, Equation 9 predicts these velocities more closely over the 0% to 45% porosity range. Indeed, over the entire porosity range, Equation 9 tends to represent a closer approximation with a minimum envelope to the data than has been postulated for Wood's equation.

Using a similar line of argument as that which led to the development of Equation 8, Equation 9 can be modified in the following way,

$$\frac{(1 + q [1 - \phi])}{\rho_s v} = \phi \left(\frac{1}{\rho_p v_p} - \frac{(1 + q_g [1 - \phi])}{\rho_g v_g} \right) + \frac{(1 + q_g [1 - \phi])}{\rho_g v_g}. \tag{10}$$

This is a semi-empirical equation based in part upon the fully validated concepts of acoustic impedance. When the velocities predicted by this equation are compared to the Leg 123 data, using the same parameters as used in Figure 6, (i.e., a sediment matrix velocity of 6500 m/s, a sediment grain density of 2.667 g/cm³, a basalt matrix velocity of 7100 m/s, a basalt grain density of 2.872 g/cm³, a pore-water velocity of 1560 m/s, a pore-fluid density of 1.0245 g/cm³, and bulk density values derived from Eq. 1), they tend to be a little too high over the higher porosity range. However, adjusting q and q_g so that both are equal to 0.22 (equivalent to a Poisson's ratio of 0.42) results in lines A and B (shown in Fig. 9) for the sediments and basalts, respectively.

The velocity values predicted by the acoustic impedance equation above achieve a much closer fit to the measured values of velocity than those predicted by the modified Wyllie-Wood equation, or indeed by any of the porosity to velocity transform models described here, over both the upper and lower porosity ranges. The adjustment to the q values in the acoustic impedance equation

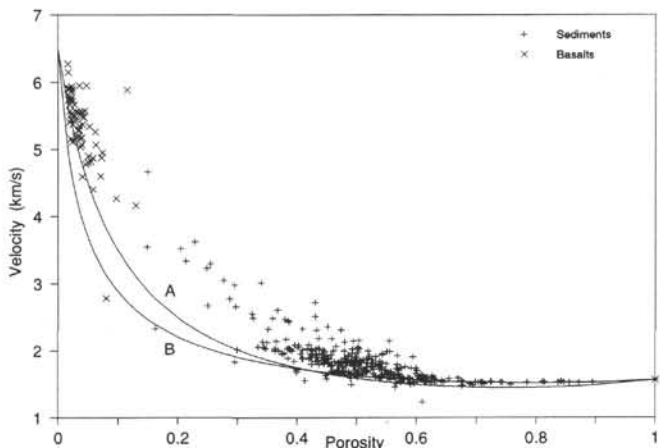


Figure 8. Acoustic impedance and Wood's emulsion equation velocity/porosity predictions.

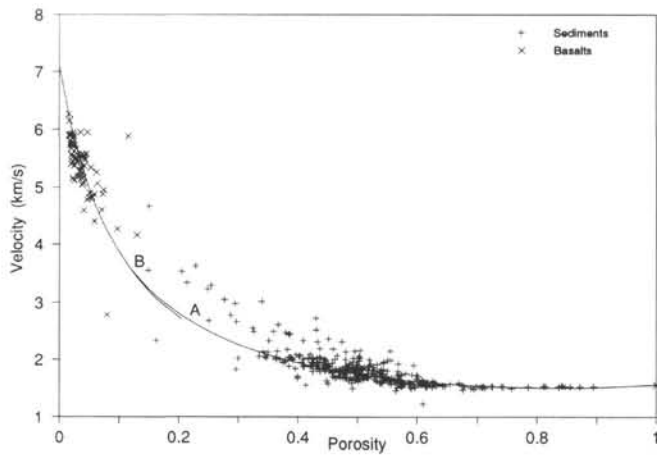


Figure 9. Velocity/porosity predictions using the modified acoustic impedance equation.

is considered acceptable because of the semi-empirical nature of Equation 10; however, the Poisson's ratio of 0.42 is still within the range of values presented in the literature for limestones and sandstones.

Of course, a more accurate representation of predicted velocities for individual samples will be obtained by using the measured values of grain and bulk densities, rather than derived values of bulk density from Equation 1 and average grain densities. However, this procedure does not give smooth curves for comparing velocity predictions of one model with those of another.

THERMAL CONDUCTIVITY RELATIONSHIPS

All thermal conductivity values determined during Leg 123 are listed in Tables 3 and 4 for Sites 765 and 766, respectively. These values are the same as those listed in the *Initial Reports* volume for Leg 123.

Although it was not practical to measure thermal conductivities and index properties for the same sample, I was able to compare predictive equations by assuming that each thermal conductivity sample would have index properties similar to the closest depth match of an index property sample. Clearly, this will introduce correlation errors, but depth mismatches averaged only 0.8 m between the two sets of core samples.

I have shown in earlier sections of this paper that satisfactory models describing relationships between porosity and other physical properties are all of the general form,

$$f_s = f_p \phi + f_g (1 - \phi),$$

where f is an appropriate function. By following a similar line of reasoning, a convincing relationship between thermal conductivity and porosity can be shown to be of the form,

$$\kappa \rho_s = \phi (\kappa_p \rho_p) + (1 - \phi) \kappa_g \rho_g, \tag{11}$$

where κ is the thermal conductivity of the sample, κ_p is the pore-fluid thermal conductivity, and κ_g is the rock-matrix thermal conductivity. Satisfactory correlations between predictions and measured values (Fig. 10) can be obtained by using thermal conductivities of both basalt and sediment matrices of 1.70 and 1.65 W/m°C, respectively (lines A and B) and a pore-fluid value of 0.55 W/m°C.

Nobes et al. (1986) used a relationship of the following form to derive thermal conductivities from porosity:

$$\kappa = \kappa_p^{\phi} \kappa_g^{(1-\phi)}. \tag{12}$$

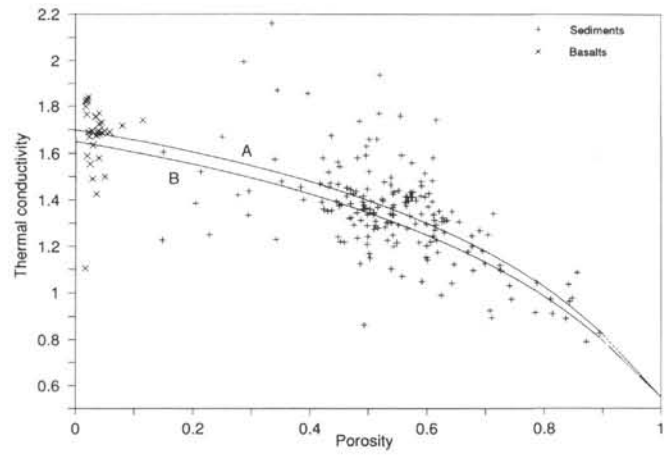


Figure 10. Thermal conductivity/porosity predictions using Equation 11.

Again, reasonably satisfactory correlations between predictions and measured values (Fig. 11) can be achieved by using corresponding matrix and pore-fluid thermal conductivities of 1.75, 2.60, and 0.70 W/m°C, respectively.

The spread of measured values of thermal conductivity as porosity decreases (due in part to the lack of correspondence between samples), leads to difficulties when deciding which of these two models is most appropriate. However, physical considerations would lead one to expect that thermal conductivity, porosity, and density express some degree of interdependence and that Equation 11 might be the more realistic. Again, by plotting the linearized forms of these two relationships, Equation 11 produces a marginally more convincing straight line than does Equation 12.

DISCUSSION AND CONCLUSIONS

The limitations of the Wyllie time average equation have been known for many years and have been re-emphasized here by comparing predicted with measured compressional-wave velocities of marine samples ranging from oozes, near to the sea/sediment interface through basement basalts. A semi-empirical acoustic impedance relationship has been developed that is shown to provide a more accurate porosity-velocity transform, using realistic material parameters, than has hitherto been possible. Because a closer correlation can be achieved with this semi-

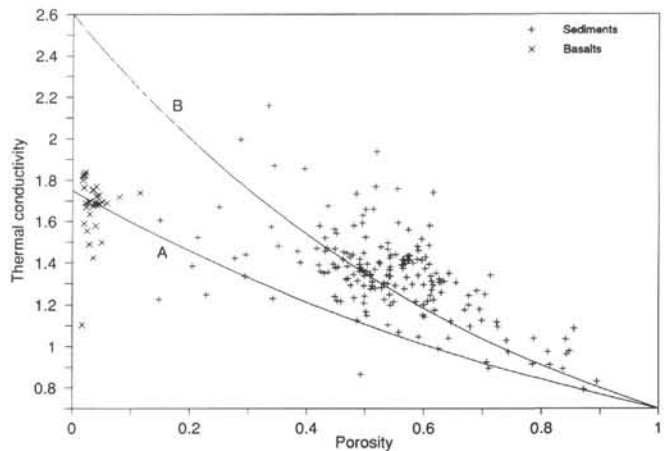


Figure 11. Thermal conductivity/porosity predictions using Equation 12.

empirical equation than with the more theoretically based modified Wyllie-Wood equation, perhaps opens to question some of the fundamental assumptions governing compressibilities of materials upon which early work was based.

I also show that a satisfactory empirical equation can be used to describe the relationships between thermal conductivity and porosity. However, the lack of direct correspondence between measured samples has precluded exploration of this relationship in more detail.

If enough is known about the lithology to provide estimates of the matrix and pore-water parameters, Equations 1, 10, and 11 enable one to describe completely the behavior of a saturated rock core in terms of compressional-wave velocity, thermal conductivity, porosity, and bulk density. If measurements of bulk density and grain density also are available, one can determine average values of some of these parameters or, alternatively, one no longer needs to assume grain densities for each sample.

ACKNOWLEDGMENTS

I wish to thank Michael Riggins, my fellow Physical Properties Specialist during Leg 123; Roland Beaussillon, who performed many of the thermal conductivity determinations; John Ludden and Felix Gradstein, the two Co-Chief Scientists; Andrew Adamson, the ODP Staff Scientist; and all the scientific party and crew of *JOIDES Resolution* during the cruise.

REFERENCES

- Anderson, R. A., 1984. Fluid and frequency effects on sonic velocities. *SPWLA Trans., 25th Logging Symp.*, Pap. AAA.
- Anderson, R. S., 1974. Statistical correlation of physical properties and sound velocity in sediments. In Hampton, L. (Ed.), *Physics of Sound in Marine Sediments*: New York and London (Plenum Press).
- Breterton, N. R., 1990. Physical properties of sediments and basalts from the Argo and Gascoyne Abyssal Plains in the Indian Ocean. *British Geol. Surv. Tech. Rep.*, WK/90/11.
- Buchan, S., Dewes, F.C.D., Jones, A.S.G., McCann, D. M., and Taylor-Smith, D., 1971. The acoustic and geotechnical properties of North Atlantic cores. *Univ. College of North Wales, Mar. Sci. Laboratories, Geol. Rep.*, 71-1.
- Castagna, J. P., Batzle, M. L., and Eastwood, R. L., 1985. Relationships between compressional-wave and shear-wave velocities in clastic silicate rocks. *Geophysics*, 50 (4):571-581.
- Collins, H. N., and Pillis, D., 1979. Some uses of functional analysis in petrophysics. *Trans., 7th Formation Evaluation Symp. Can. Well Logging Soc.*, Pap. E.
- Domenico, S. N., 1984. Rock lithology and porosity determinations from shear and compressional-wave velocity. *Geophysics*, 49(8):1188-1195.
- Dresser Atlas., 1982. *Well Logging and Interpretation Techniques*: Houston (Dresser Atlas).
- Fulthorpe, C. S., and Schlanger, S. O., 1989. *In situ* acoustic properties of pelagic carbonate sediments on the Ontong Java Plateau. *J. Geophys. Res.*, 94:4025-4032.
- Gardner, G.H.F., Gardner, L. W., and Gregory, A. R., 1974. Formation velocity and density—the diagnostic basics for stratigraphic traps. *Geophysics*, 39(6):770-780.
- Hamilton, E. L., 1971. Elastic properties of marine sediments. *J. Geophys. Res.*, 76(2):579-604.
- _____, 1974. Prediction of deep-sea sediment properties: state-of-the-art. In Inderbitzen, A. L. (Ed.), *Deep-Sea Sediments*: New York and London (Plenum Press).
- Han, D., Nur, A., and Morgan, D., 1986. Effects of porosity and clay content on wave velocities in sandstone. *Geophysics*, 51(11):2093-2107.
- Hearst, J. R., and Nelson, P. H., 1985. *Well Logging for Physical Properties*: New York (McGraw-Hill).
- Jackson, P. D., Baria, R., and McCann, D. M., 1981. Geotechnical assessment of superficial marine sediments using in-situ geophysical probes. *Ocean Management*, 7:189-209.
- Ludden, J. N., Gradstein, F. M., et al., 1990. *Proc. ODP, Init. Repts.*, 123: College Station, TX (Ocean Drilling Program).
- McCann, C., 1968a. An investigation of the acoustic properties of natural materials [Unpubl. Ph.D. dissert.], Univ. of Wales, Bangor.
- McCann, D. M., 1968b. The acoustic properties of North Atlantic cores [Unpubl. Ph.D. dissert.], Univ. of Wales, Bangor.
- Nafe, J. E., and Drake, C. L., 1957. Variation with depth in shallow and deep water marine sediments of porosity, density and the velocities of compressional- and shear-waves. *Geophysics*, 22(3):523-552.
- Nobes, D. C., Villinger, H., Davis, E. E., and Law, L. K., 1986. Estimation of marine sediment bulk physical properties at depth from seafloor geophysical measurements. *J. Geophys. Res.*, 91:14033-14043.
- ODP Leg 123 Shipboard Scientific Party, 1989a. Ocean Drilling Program—the birth of the Indian Ocean. *Nature*, 337:506-507.
- ODP Leg 123 Shipboard Scientific Party, 1989b. ODP investigates Indian Ocean origins. *Geotimes*, 34(3):16-19.
- Rafavich, F., Kendall, C.H.St.C., and Todd, T. P., 1984. The relationship between acoustic properties and the petrographic character of carbonate rocks. *Geophysics*, 10:1622-1636.
- Raiga-Clemenceau, J., Martin, J. P., and Nicoletis, S., 1988. The concept of acoustic formation factor for more accurate porosity determination from sonic transit time data. *The Log Analyst*, Jan-Feb, 1988.
- Raymer, L. L., Hunt, E. R., and Gardner, J. S., 1980. An improved sonic transit time-to-porosity transform. *SPWLA Trans., 21st Logging Symp.*, Pap. P.
- Schlumberger, 1972. *Log Interpretation Principles*: New York (Schlumberger).
- Shumway, G., 1960. Sound and absorption studies of marine sediments by a resonance method, parts I and II. *Geophysics*, 25(2):451-467, and (3):659-682.
- Stam, B., Gradstein, F. M., Lloyd, P., and Gillis, D., 1987. Algorithms for porosity and subsidence history. *Comput. Geosci.*, 13(4):317-349.
- Taylor-Smith, D., 1974. Acoustic and mechanical loading of marine sediments. In Hampton, L. (Ed.), *Physics of Sound in Marine Sediments*: New York and London (Plenum Press).
- Wilkens, R. H., Simmons, G., Wissler, T. M., and Caruso, L., 1986. The physical properties of a set of sandstones - part III. The effects of fine-grained pore filling material on compressional-wave velocity. *Int. J. Rock Mech. Mineral. Sci. Geomech. Abstr.*, 4:313-325.
- Wood, A. B., 1941. *A Textbook of Sound*: New York (Macmillan).
- Wyllie, M.R.J., Gregory, A. R., and Gardner, L. W., 1956. Elastic wave velocities in heterogeneous and porous media. *Geophysics*, 21(1):41-70.
- _____, 1958. An experimental investigation of factors affecting elastic wave velocities in porous media. *Geophysics*, 23(3):459-493.
- Yale, D. P., 1985. Recent advances in rock physics. *Geophysics*, 50(12):2480-2491.

Date of initial receipt: 15 May 1990

Date of acceptance: 6 May 1991

Ms 123B-131

Table 3. Thermal conductivity data, Site 765.

Core, section, interval (cm)	Depth (mbsf)	Thermal conductivity (W/m · °C)
Sediments		
123-765A-1H-2, 40	1.50	0.812
A-1H-3, 40	3.00	1.064
A-1H-4, 40	4.50	0.791
A-1H-5, 40	6.00	1.118
765B-1H-1, 40	0.00	0.777
B-1H-2, 40	1.50	0.846
B-1H-3, 40	3.00	0.892
B-1H-5, 40	6.00	1.054
B-2H-1, 40	9.30	0.973
B-2H-3, 40	12.30	0.973
B-2H-5, 40	15.30	0.874
B-2H-6, 40	16.80	0.911
B-3H-1, 40	18.80	1.030
B-3H-2, 40	20.30	0.896
B-3H-3, 40	21.80	0.837
B-3H-4, 40	23.30	1.035
B-4H-1, 50	28.50	0.895
B-4H-3, 50	31.50	1.118
B-4H-4, 50	33.00	0.916
B-4H-6, 50	36.00	0.963
B-5H-1, 40	38.10	0.891
B-5H-3, 40	41.10	1.115
B-5H-5, 40	44.10	1.095
B-5H-6, 40	45.60	1.151
B-6H-1, 40	47.80	1.053
B-6H-2, 40	49.30	1.213
B-6H-3, 40	50.80	0.926
B-6H-3, 40	50.80	0.926
B-6H-6, 40	55.30	1.040
B-7H-1, 40	57.40	1.126
B-7H-3, 40	60.40	1.231
B-7H-4, 40	61.90	0.990
B-7H-6, 40	64.90	1.350
B-8H-2, 40	68.60	1.125
B-8H-4, 40	71.60	1.123
B-8H-5, 40	73.10	1.122
B-9H-1, 45	76.80	1.225
B-9H-3, 45	79.80	1.341
B-9H-4, 45	81.30	1.259
B-9H-6, 45	84.30	1.245
B-10H-1, 40	86.40	1.306
B-10H-3, 40	89.40	1.176
B-10H-5, 40	92.40	1.328
B-10H-6, 40	93.90	1.174
B-11H-1, 40	96.00	1.041
B-11H-3, 40	99.00	1.293
B-11H-5, 40	102.00	1.362
B-11H-6, 40	103.50	1.283
B-13H-1, 60	115.20	1.312
B-13H-3, 60	118.20	1.351
B-13H-5, 60	121.20	1.199
B-13H-6, 60	122.70	1.298
B-15H-1, 51	134.50	1.371
B-15H-3, 51	137.50	1.372
B-15H-5, 51	140.50	1.340
B-15H-6, 51	142.00	1.428
B-16H-2, 50	145.70	1.307
B-16H-3, 50	147.20	1.393
B-16H-5, 50	150.20	1.242
B-16H-6, 50	151.70	1.219
B-18H-2, 50	165.10	1.278
B-18H-3, 50	166.00	1.337
B-18H-5, 50	169.00	1.433
B-18H-7, 50	172.00	1.244
B-19X-2, 30	174.80	1.375
B-19X-3, 30	176.30	1.250
B-19X-4, 30	177.80	2.146
B-19X-5, 30	179.30	1.337
B-20X-2, 37	184.50	1.113
B-20X-3, 37	186.00	1.338
B-20X-5, 37	189.00	1.396
B-20X-6, 37	190.50	1.337
B-21X-2, 50	194.20	1.435
B-21X-3, 50	195.70	1.276

Table 3 (continued).

Core, section, interval (cm)	Depth (mbsf)	Thermal conductivity (W/m · °C)
Sediments (Cont.)		
123-765B-21X-4, 50	197.20	1.414
B-21X-5, 50	198.70	1.363
B-22X-1, 36	202.40	1.428
B-22X-3, 36	205.40	1.217
B-22X-4, 36	206.90	1.441
B-22X-5, 36	208.40	1.290
B-23X-1, 110	212.10	1.480
B-23X-1, 30	212.10	1.513
B-23X-2, 110	213.60	1.318
B-23X-2, 30	213.60	1.466
B-24X-1, 40	221.80	1.425
B-24X-2, 40	223.30	1.401
B-24X-3, 40	224.80	1.296
B-24X-4, 40	226.30	1.346
B-25X-1, 50	231.50	1.282
B-26X-1, 50	241.20	1.304
B-26X-3, 50	244.20	1.768
B-26X-4, 50	245.70	1.431
B-27X-1, 30	250.90	1.325
B-27X-2, 30	252.40	1.260
B-27X-3, 50	253.90	1.430
B-27X-3, 30	253.90	1.290
B-28X-1, 60	260.60	1.237
B-28X-1, 33	260.60	1.413
B-28X-2, 33	262.10	1.051
B-28X-3, 33	263.60	1.349
B-29X-1, 50	270.20	1.362
B-29X-1, 90	270.20	1.389
B-29X-2, 10	271.70	1.416
B-30X-1, 30	279.90	1.483
B-31X-1, 60	289.60	1.252
B-31X-2, 60	291.10	1.439
B-31X-3, 60	292.60	1.536
B-31X-4, 60	294.10	1.369
B-32X-1, 80	299.30	1.407
B-32X-1, 120	299.30	1.638
B-32X-2, 80	300.80	1.739
B-32X-3, 80	302.30	1.321
B-33X-1, 50	309.00	1.293
B-33X-2, 50	310.50	1.417
B-33X-4, 50	313.50	1.387
B-33X-5, 50	315.00	1.241
B-34X-1, 30	318.70	1.235
B-34X-2, 46	320.20	1.581
B-35X-1, 30	328.30	1.453
B-36X-1, 80	337.90	1.478
B-36X-2, 60	339.40	1.467
B-36X-3, 50	340.90	1.628
B-37X-1, 60	347.50	1.218
B-37X-2, 40	348.70	1.455
B-38X-1, 60	357.10	1.416
B-39X-1, 60	366.70	1.936
B-40X-1, 10	376.40	1.282
B-41X-1, 15	386.00	1.230
765C-2R-1, 31	359.60	1.510
C-2R-1, 31	359.60	1.530
C-3R-2, 34	370.80	1.410
C-3R-2, 34	370.80	1.380
C-4R-1, 120	379.00	1.350
C-4R-1, 120	379.00	1.370
C-5R-2, 79	390.10	1.350
C-5R-2, 91	390.10	1.430
C-5R-2, 110	390.10	1.244
C-5R-2, 91	390.10	1.360
C-5R-2, 96	390.10	1.503
C-6R-1, 91	398.30	1.590
C-6R-1, 91	398.30	1.570
C-7R-1, 18	408.00	1.390
C-7R-1, 18	408.00	1.320
C-8R-3, 8	420.70	1.250
C-8R-3, 8	420.70	1.310
C-9R-3, 88	430.30	1.340
C-9R-3, 88	430.30	1.330
C-10R-4, 38	441.00	1.300

Table 3 (continued).

Core, section, interval (cm)	Depth (mbsf)	Thermal conductivity (W/m · °C)
Sediments (Cont.)		
123-765C-10R-4, 38	441.00	1.280
C-11R-3, 102	449.00	2.100
C-11R-3, 102	449.00	1.990
C-12R-5, 69	461.20	1.720
C-12R-5, 69	461.20	1.630
C-13R-2, 131	466.10	1.600
C-13R-2, 131	466.10	1.610
C-13R-3, 0	467.60	1.290
C-13R-3, 0	467.60	1.472
C-13R-3, 0	467.60	1.440
C-14R-1, 35	474.10	1.490
C-14R-1, 35	474.10	1.420
C-16R-1, 108	493.20	1.520
C-16R-1, 108	493.20	1.600
C-17R-1, 14	502.40	1.200
C-17R-1, 14	502.40	1.240
C-18R-2, 134	513.40	1.680
C-18R-2, 134	513.40	1.640
C-23R-5, 5	565.70	2.120
C-23R-5, 5	565.70	2.000
C-24R-3, 16	572.30	1.870
C-24R-3, 16	572.30	1.840
C-25R-1, 21	579.00	1.860
C-25R-1, 21	579.00	1.880
C-28R-1, 73	607.00	1.070
C-28R-1, 73	607.00	1.070
C-29R-2, 45	617.97	1.149
C-29R-4, 44	621.02	1.366
C-29R-6, 43	624.17	1.275
C-30R-2, 64	627.39	1.246
C-30R-2, 64	627.39	1.172
C-30R-3, 38	628.85	1.263
C-30R-3, 38	628.85	1.409
C-30R-6, 51	633.29	1.163
C-30R-6, 51	633.29	1.394
C-31R-1, 98	635.30	1.358
C-31R-1, 31	635.30	1.094
C-31R-2, 47	636.71	1.564
C-31R-3, 101	638.18	1.257
C-31R-4, 58	639.61	1.380
C-33R-2, 30	656.18	1.206
C-33R-2, 60	656.18	1.275
C-37R-3, 101	696.00	1.400
C-37R-3, 101	696.00	1.380
C-38R-5, 5	708.50	1.380
C-38R-5, 5	708.50	1.340
C-38R-5, 5	708.50	1.360
C-39R-3, 42	714.70	1.410
C-39R-3, 42	714.70	1.380
C-40R-2, 95	722.40	1.450
C-40R-2, 95	722.40	1.490
C-42R-3, 16	742.80	1.380
C-42R-3, 16	742.80	1.370

Basalts

765D-1R-1, 52	948.42	1.735
D-1R-1, 52	948.42	1.725
D-1R-2, 52	949.92	1.725
D-2R-2, 0	956.09	1.105
D-2R-3, 95	958.11	1.670
D-3R-1, 33	964.73	1.695
D-4R-1, 30	974.00	1.610
D-5R-1, 133	984.53	1.675
D-5R-5, 29	988.45	1.755
D-5R-7, 129	992.29	1.760
D-6R-1, 0	992.40	1.675
D-7R-1, 81	1002.81	1.690
D-8R-1, 28	1011.78	1.770
D-9R-1, 72	1021.62	1.840
D-9R-1, 72	1021.62	1.840
D-10R-1, 64	1030.84	1.580
D-11R-1, 90	1040.30	1.590
D-12R-1, 26	1045.36	1.690

Table 3 (continued).

Core, section, interval (cm)	Depth (mbsf)	Thermal conductivity (W/m · °C)
Basalts (Cont.)		
123-765D-15R-1, 55	1073.55	1.555
D-17R-2, 103	1094.16	1.695
D-18R-1, 10	1101.20	1.830
D-19R-1, 114	1111.44	1.500
D-20R-2, 71	1121.71	1.635
D-21R-1, 113	1130.13	1.755
D-22R-1, 15	1138.75	1.690
D-23R-2, 20	1149.50	1.725
D-24R-4, 42	1161.32	1.740
D-25R-1, 125	1167.75	1.765
D-26R-2, 92	1178.42	1.425
D-27R-2, 40	1186.95	1.725

Table 4. Thermal conductivity data, Site 766.

Core, section, interval (cm)	Depth (mbsf)	Thermal conductivity (W/m · °C)
Sediments		
123-766A-1R-1, 110	1.1	1.407
A-1R-2, 40	1.9	1.095
A-1R-3, 40	3.4	1.096
A-2R-1, 50	8.2	1.228
A-2R-2, 50	9.76	1.268
A-2R-3, 55	11.31	1.137
A-2R-5, 55	14.31	1.200
A-3R-2, 45	19.25	1.270
A-3R-3, 45	20.75	1.515
A-3R-4, 45	22.25	1.593
A-3R-CC, 10	26.40	1.529
A-4R-1, 60	27.60	1.515
A-4R-2, 60	29.10	1.374
A-5R-3, 60	40.30	1.480
A-5R-6, 30	44.50	1.412
A-6R-4, 60	51.40	1.350
A-7R-1, 40	56.40	1.089
A-7R-2, 40	57.90	1.425
A-7R-4, 33	60.83	1.413
A-7R-7, 30	65.30	1.413
A-8R-1, 50	66.20	1.412
A-8R-2, 44	67.64	1.439
A-9R-1, 60	75.90	1.417
A-9R-4, 60	80.40	1.460
A-10R-1, 70	85.70	1.340
A-10R-3, 50	88.50	1.479
A-11R-3, 40	98.10	1.630
A-11R-4, 40	99.60	1.735
A-12R-1, 40	104.70	1.659
A-12R-2, 40	106.20	1.505
A-13R-1, 40	114.30	1.742
A-13R-3, 40	117.30	1.759
A-14R-1, 40	124.00	1.512
A-14R-2, 40	125.50	1.433
A-15R-2, 101	135.71	0.977
A-15R-4, 90	138.60	1.581
A-16R-2, 120	145.60	1.367
A-16R-5, 54	149.44	1.341
A-17R-2, 70	154.70	1.436
A-17R-5, 38	158.88	1.391
A-17R-7, 20	161.70	1.294
A-18R-1, 47	162.57	1.341
A-18R-3, 34	165.44	1.276
A-18R-6, 38	169.98	1.384
A-19R-1, 78	172.48	1.396
A-19R-3, 43	175.13	1.249
A-19R-5, 32	178.02	1.216
A-20R-1, 98	182.38	1.426
A-20R-2, 40	183.30	1.439

Table 4 (continued).

Core, section, interval (cm)	Depth (mbsf)	Thermal conductivity (W/m · °C)
Sediments		
123-766A-20R-4, 30	186.20	1.095
A-21R-1, 43	191.43	1.472
A-21R-2, 82	193.32	1.445
A-24R-1, 110	221.00	1.669
A-25R-1, 23	229.83	1.481
A-26R-2, 70	241.50	1.226
A-26R-3, 56	242.86	1.169
A-27R-1, 114	250.04	0.864
A-27R-2, 51	250.91	1.103
A-28R-2, 53	260.63	1.242
A-28R-4, 60	263.70	1.332
A-29R-1, 80	269.10	1.142
A-29R-3, 60	271.90	1.202
A-30R-2, 80	280.20	1.048
A-30R-4, 40	282.80	1.152
A-36R-1, 52	336.32	1.346
A-36R-1, 115	336.95	1.374
A-36R-2, 16	337.46	1.399
A-37R-1, 62	346.12	1.477
A-38R-1, 75	355.85	1.574
A-38R-3, 68	358.78	1.543
A-39R-1, 78	365.58	1.351
A-39R-3, 71	368.51	1.380
A-41R-1, 116	385.36	1.345
A-42R-2, 35	395.65	1.292
A-42R-4, 35	398.65	1.325
A-42R-4, 38	398.68	1.444
A-43R-2, 35	405.35	1.300
A-43R-4, 35	408.35	1.592
A-44R-2, 50	415.20	1.465
A-44R-6, 50	421.20	1.447
A-45R-3, 50	426.30	1.522
A-45R-7, 30	432.10	1.404
A-46R-3, 50	436.04	1.422
A-46R-6, 50	440.54	1.303
A-47R-2, 50	444.20	1.339
A-47R-6, 50	450.20	1.125
A-49R-4, 77	466.77	1.490
Basalts		
A-50R-3, 48	474.50	1.685
A-51R-3, 86	484.21	1.680
A-52R-1, 79	490.69	1.695
A-52R-3, 0	492.97	1.820
A-53R-3, 45	502.15	1.825
A-54R-4, 67	512.93	1.800
A-55R-7, 136	527.02	1.835